

PHYSICAL CONDITIONS IN ULTRA FAST OUTFLOWS IN AGN

S.B. KRAEMER,¹ F.TOMBESI,^{2,3,4} AND M.C. BOTTORFF⁵

¹*Institute for Astrophysics and Computational Sciences, Dept. of Physics, The Catholic University of America, Washington, DC 20064; kraemer@cua.edu*

²*Department of Astronomy, University of Maryland, College Park, MD 20742, USA; ftombesi@astro.umd.edu*

³*NASA/Goddard Space Flight Center, Code 662, Greenbelt, MD 20771, USA*

⁴*Department of Physics, University of Rome “Tor Vergata”, Via della Ricerca Scientifica 1, I-00133 Rome, Italy*

⁵*Department of Physics, Southwestern University, Georgetown TX, 78626, USA; bottorfm@southwestern.edu*

ABSTRACT

XMM-*Newton* and *Suzaku* spectra of AGN have revealed highly ionized gas, in the form of absorption lines from H-like and He-like Fe. Some of these absorbers, “Ultra Fast Outflows (UFOs)”, have radial velocities of up to 0.25c. We have undertaken a detailed photo-ionization study of high-ionization Fe absorbers, both UFOs and non-UFOs, in a sample of AGN observed by XMM-*Newton*. We find that the heating and cooling processes in UFOs are Compton-dominated, unlike the non-UFOs. Both types are characterized by Force Multipliers on the order of unity, which suggests that they cannot be radiatively accelerated in sub-Eddington AGN, unless they were much less ionized at their point of origin. However, such highly ionized gas can be accelerated via a Magneto-Hydrodynamic (MHD) wind. We explore this possibility by applying a cold MHD flow model to the UFO in the well-studied Seyfert galaxy, NGC 4151. We find that the UFO can be accelerated along magnetic streamlines anchored in the accretion disk. In the process, we have been able to constrain the magnetic field strength and the magnetic pressure in the UFO and have determined that the system is not in magnetic/gravitational equipartition. Open questions include the variability of the UFOs and the apparent lack of non-UFOs in UFO sources.

Keywords: accretion, accretion disks, galaxies: active, X-rays: galaxies

1. INTRODUCTION

According to the standard paradigm, Active Galactic Nuclei (AGN) are powered by accretion of matter onto a supermassive black hole (SMBH). The reservoir of fuel is thought to be an accretion disk surrounding the black hole, from which outflowing winds may arise (e.g., Rees 1987). More than 50% of Seyfert 1 galaxies, relatively local ($z < 0.1$), modest luminosity ($L_{bol} < 10^{45}$ erg s $^{-1}$) AGN, show intrinsic X-ray and UV absorption (Crenshaw et al. 2003), suggesting that the absorbers have global covering factors $C_g \sim 0.5$. Blue-shifted absorption lines in their UV (Crenshaw et al. 1999) and X-ray (Kaastra et al. 2000; Kaspri et al. 2000) spectra reveal significant outflow velocities (up to -4000 km s $^{-1}$, Dunn et al. 2007). The inferred mass-loss rates typically exceed the accretion rates needed to produce the observed luminosities of AGN (e.g., Crenshaw & Kraemer 2012). Hence, mass outflows are a critical component in the structure, energetics, and evolution of AGN. Specifically, the relation between bulge mass and black hole mass is thought to be regulated by AGN outflows, i.e., “AGN feedback” (Begelman 2004). Various acceleration mechanisms have been proposed for these outflows, specifically: radiative driving (e.g., Murray et al. 1995), thermal winds (Begelman et al. 1983), and magneto-hydrodynamic (MHD) flows (e.g., Blandford & Payne 1982; Fukumura et al. 2010; Chakravorty et al. 2016).

If AGN-driven outflows are an important feedback mechanism, they must be energetic enough to clear the gas in the bulge of the host galaxy and quench star-formation. Their strength can be expressed in the form of “Kinetic Luminosity”, $L_{KE} = \frac{1}{2} \dot{M}_{out} v_r^2$, where the mass outflow rate $\dot{M}_{out} = 4\pi r N_H \mu m_p C_g v_r$, and r is radial distance of the gas, N_H is column density, μ is the mean atomic mass per proton ($= 1.4$ for so-

lar abundances), m_p is the proton mass, C_g is the global covering fraction of the gas, and v_r is radial velocity. For effective feedback, $L_{KE} \sim 0.5\% - 5\%$ of L_{bol} , the bolometric luminosity of the AGN (Hopkins & Elvis 2010; King & Pounds 2015). Since $L_{KE} \propto v_r^3$, the amount of kinetic energy deposited into the host galaxy rises quite rapidly with velocity. One caveat is that the theoretical models for feedback require that the AGNs are radiating close to their Eddington limit (e.g., King & Pounds 2015), or $L_{bol}/L_{Edd} \sim 1$ (but see below).

Crenshaw & Kraemer (2012) and Crenshaw et al. (2015) have explored the impact of feedback from outflowing UV and X-ray absorbers and optical emission-line gas, in the Narrow Line Region (NLR), of a sample of nearby Seyfert galaxies. For half of the sample, $L_{KE} \leq 0.5\% L_{bol}$, and most of these sources are significantly sub-Eddington, hence cannot effectively drive feedback. In their study of the Seyfert 2 galaxy, Mrk 573, Fischer et al. (2017) find that, while the AGN is radiating at near the Eddington limit, gas is not being radiatively accelerated at radial distances $\gtrsim 1$ kpc. These results call into question the effectiveness of AGN feedback, at least in the local Universe.

However, there are more extreme phenomena, so-called ultra-fast outflows (UFO), which are defined as massive, highly ionized, modestly relativistic outflows. They are identified by narrow Fe K-shell blueshifted absorption lines from Fe XXV/XXVI, with $v_r \sim 0.03 - 0.3c$ (Chartas, Brandt, & Gallagher 2003; Pounds et al. 2003; Reeves, O’Brien, & Ward 2003; Tombesi et al. 2010). The lines are quite prominent, with EWs in the range 10 - 100 eV (Tombesi et al. 2010). UFOs might drive a significant amount of mass and, most importantly, energy outwards, and therefore could be a critical component of AGN feedback. Photoionization modeling of UFOs predicts column densities on the order of $N_H \sim$

$10^{23} - 10^{24} \text{ cm}^{-2}$, and very high ionization, in the range of $\log Xi^1 \sim 3 - 6$. There are also highly ionized absorption components that do not fit within the UFO parameterization, showing $\log (Xi) < 3$ and $v_r < 0.03c$, which are classified as non-UFOs (Tombesi et al. 2010).

Previous studies (Cappi et al. 2006; Tombesi et al. 2010, 2011, 2012, 2014) have identified UFOs in archival *XMM-Newton* observations of samples of both radio-quiet and radio-loud galaxies. Many of them were later confirmed in the same sources in *Suzaku* spectra by Gofford et al. (2013, 2015). These authors have derived qualitative information on the UFO spectral characteristics, kinematics and possible location. Tombesi et al. (2012) noted that there seem to be tight correlations between the location of UFO with respect to the SMBH, and the ionization state, column density and velocity of the outflowing gas. The high state of ionization combined with relativistic velocities suggests an origin in the inner accretion disk. Furthermore, King & Pounds (2015) argue that UFOs are required for AGN feedback. For example, based on 3-dimensional hydrodynamic simulations, Wagner, Umemura, & Bicknell (2013) suggested that UFOs lose their dependence on opening angle upon their initial interaction with the interstellar medium of the host galaxy, hence produce larger-scale feedback than lower-velocity winds (also, see Asahina, Nomura, & Oshuga (2017)).

Despite intense study, the origin and acceleration mechanism of UFOs are still unclear. There is evidence for variability on timescales of years (Reeves et al. 2008; Pounds & Reeves 2009;

¹ the ionization parameter $Xi = L_{\text{ion}}/n_H r^2$, where L_{ion} is the ionizing luminosity of the AGN, n_H is the hydrogen number density, and r is radial distance (Tarter et al. 1969). We use Xi rather than the Greek letter ξ to avoid confusion with the scaling parameter used for self-similar MHD solutions.

Cappi et al. 2009), or as short as days, as in the case of Mrk 766 (Tombesi et al. 2010), which suggests an origin close to the AGN (although it is possible that the variability is due to instabilities within the absorbers (e.g., Takeuchi, Ohsuga, & Mineshiga 2013)). Gofford et al. (2013) and King & Pounds (2015) argue for acceleration by radiation. However, given their high ionization state (Tombesi et al. 2011; Gofford et al. 2013), this can only occur via electron scattering, which is not likely as most AGN with UFO detections are radiating at a small fraction of Eddington, unless there are multiple scatterings, which are not feasible given the UFO column densities (e.g., Tombesi et al. 2011).

On the other hand, it has been suggested that radiative acceleration of UFOs via UV line-driving is possible if they were in a sufficiently low ionization state near their launch points (e.g., Hagino et al. 2015, 2017; Nomura et al. 2016; Nomura & Ohsuga 2017). In this scenario, as the UFOs flow outwards, they become increasingly ionized, until only H- and He-like Fe lines can be detected. These models predict that fast flows can be generated in sub-Eddington sources.

However, it is also plausible that there is a non-radiative means of acceleration, specifically through a magnetohydrodynamic (MHD) wind (e.g., Fukumura et al. 2010, 2014; Chakravorty et al. 2016). In this paper, we explore this possibility as follows. First, we perform a photoionization modeling analysis of the UFOs, and non-UFOs, studied by Tombesi et al. (2010). In doing so, we obtain constraints on physical conditions within the absorbers, including: density, electron temperature, and the heating and cooling processes at work. We then review the cold MHD flow model proposed by Blandford & Payne (1982, hereafter BP82). Finally, in the case of NGC 4151, a Seyfert galaxy for

which we have tight constraints on black hole mass, luminosity, and inclination, we show that the UFO could be part of an MHD-driven out-flow.

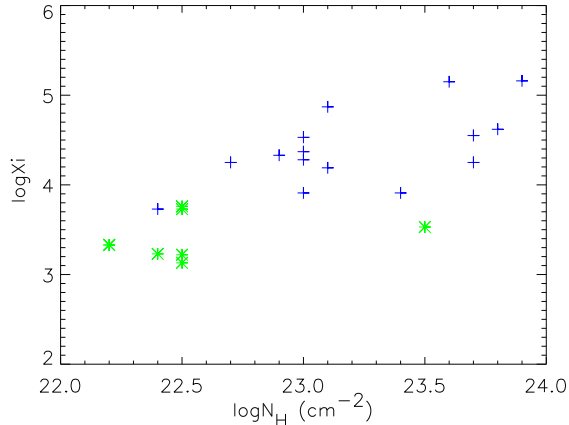


Figure 1. Log Ξ versus N_H , for the photo-ionization models discussed in Section 2; blue crosses, UFOs; green asterisks, non-UFOs. These results show that the UFOs and non-UFO occupy different regions of parameter space.

2. PHOTIONIZATION MODELS

2.1. Model Inputs

In order to characterize the absorbers, Tombesi et al. (2011) and Gofford et al. (2015) fit spectra using photoionization models generated with XSTAR (Kallman et al. 2004). From the models, they were able to constrain the range in ionization parameter and column density of the individual absorbers. As noted above, the models were parameterized in terms of Ξ .

Our principle goal is to derive the physical conditions within the absorbers. To do so, we generated photo-ionization models using Cloudy (Ferland et al. 2013), from which we were able to constrain quantities such as electron temperature, T_e , relative contributions to heating and

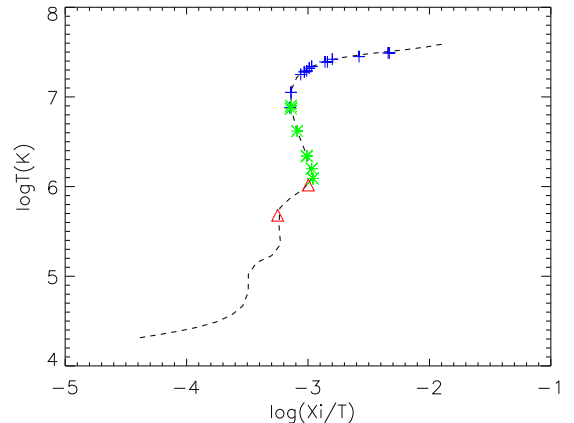


Figure 2. Thermal Stability(S-Curve) for the photo-ionization models; same as above with red triangles showing two states of the highest ionization warm absorber in NGC 4151 (“XHIGH”; Couto et al. (2016)). Note that the three types of absorbers occupy different regions of the S-curve, with the UFOs primarily on the flat, Compton-dominated section.

cooling, including Compton processes, and the “Force Multiplier (FM)”, the ratio of the total photo-absorption cross-section to the Thomson cross-section, in a physically self consistent manner. Models were optimized to match the derived Fe XXV and Fe XXVI column densities. These were determined from the the line Equivalent Width values reported in Table A.2 of Tombesi et al. (2010) using the curve of growth analysis described in Tombesi et al. (2011). We used only lines with an unambiguous identification as Fe XXV or Fe XXVI. We assumed line broadening due to a turbulent velocity of 1000 km s^{-1} and 3000 km s^{-1} for those associated with non-UFOs and UFOs, respectively. This is consistent with the upper limits obtained from the spectral fits in their Table 3. However, the broadening may, in fact, be due to velocity gradients along the line-of-sight through the absorbers, rather than micro-turbulence, a point we will revisit in Section 3.2.2. Therefore, we

did not include micro-turbulence in the Cloudy models.

The model results depend on the choice of input parameters, specifically: the spectral shape of the incident radiation or spectral energy distribution (SED), the radial distances of the emission-line gas with respect to the central source, n_{H} , and column density (N_{H}) of the gas, and its chemical composition. We assumed an SED similar to that used by Tombesi et al. (2011), in the form of a power law $F_{\nu} = K \nu^{-\alpha}$, with $\alpha = 1.0$ for $1.4 \times 10^{-4} \text{ eV} < h\nu < 100 \text{ keV}$, with exponential cutoffs above and below the limits. This SED is simpler than the broken power-law (e.g., Laor et al. 1997) that we have used in our modeling of Seyfert spectra (see Couto et al. 2016), but its use maintains consistency with the previous UFO analysis. As in our most recent warm absorber studies (e.g., Couto et al. 2016), we have assumed roughly 1.5 times solar elemental abundances (e.g., Asplund et al. 2005) as follows (in logarithm, relative to H, by number): He: -1.00 , C: -3.47 , N: -3.92 , O: -3.17 , Ne: -3.96 , Na: -5.76 , Mg: -4.48 , Al: -5.55 , Si: -4.51 , P: -6.59 , S: -4.82 , Ar: -5.60 , Ca: -5.66 , Fe: -4.4 , and Ni: -5.78 .

Ionic column densities were fit by adjusting Xi and N_{H} within the constraints determined by Tombesi et al. (2011). For a given Xi , n_{H} is a function of radial distance, r , and the ionizing luminosity, L_{ion} ; for the latter, we assumed the values from Tombesi et al. (2012). We set the upper limits for the radial distance by requiring that the physical depth, Δr , not exceed r , or $\Delta r/r < 1$. Noting that $\Delta r = N_{\text{H}}/n_{\text{H}}$, from the definition of Xi we obtain the expression $r \geq L_{\text{ion}}/(Xi N_{\text{H}})$. Then, by substituting this back into the definition of Xi , $n_{\text{H}} \leq Xi N_{\text{H}}^2/L_{\text{ion}}$.

2.2. Model Results

Model parameters are listed in Table 1 and predicted Fe XXV and Fe XXVI column densities, compared with the measured values, are shown in Table 2.² The model-predicted ionic column densities are all within a factor of 2 of the measured values, which we deem sufficiently accurate given uncertainties in the iron abundance. As shown in Table 1, Cloudy models predict that both UFOs and non-UFOs have large columns, $N_{\text{H}} \sim 10^{22-24} \text{ cm}^{-2}$, of highly ionized ($\log Xi = 3.13 - 5.16$) gas. However, there is a difference between the two classes. Non-UFOs generally possess smaller N_{H} and Xi , as is shown clearly in Figure 1. The one outlier among non-UFOs, in terms of N_{H} , is ESO 323-G77. This is due to the fact that the Fe XXV and Fe XXVI column densities in this object are quite large (see Table 2). For the UFOs, the model prediction for the first observation of Mrk 766 places it with the non-UFOs in Figure 1. However, the Fe XXVI column densities are nearly the same in both observations, there may be some uncertainty in the range in N_{H} (see Tombesi et al. 2011).

As shown in Table 1, Compton heating is the dominant mechanism for UFOs, with cooling due to Compton and free-free processes. For non-UFOs, while Compton heating can sometimes dominate, heating via ionization becomes important, and cooling via emission-lines dominates for the lowest ionization cases, e.g., NGC 3783. The difference in heating and cooling processes among UFOs and non-UFOs is clearly illustrated in a thermal stability plot (“S-Curve”; Figure 2), in which the UFOs lie primarily on the flat Compton-dominated sec-

² We were not able to obtain a satisfactory model-fit for objects with only Fe XXV-detected UFOs, 1H0419-577, NGC 7582, and PG 1211+143, or the second observation of NGC 4051, for which the measured Fe XXVI column was inconsistent with the constraint on N_{H} from Tombesi et al. (2011).

tion. The non-UFOs are found along the negatively sloped portion of the curve, suggesting that they are thermally unstable (e.g., [Bottorff et al. 2000](#)). However, the shape of the vertical section of the S-Curve depends on the SED, which is unusually flat for these models (see above) and the atomic data, which may be incomplete for M- and L-shell iron ions which dominate cooling in these conditions (e.g., [Kraemer et al. 2015](#)). Also, as suggested by [Bottorff et al. \(2000\)](#), a sufficiently strong magnetic field could stabilize the gas (see their Appendix A3). At a minimum, this result illustrates the difference in the physical conditions within the non-UFOs as compared to the UFOs. In Figure 2 we have also plotted the position of the highest ionization component of warm absorption in NGC 4151, “XHIGH” (see [Couto et al. 2016](#)), modeled for two continuum flux states. As suggested by [Tombesi et al. \(2011\)](#), there is a continuum between UFOs, non-UFOs, and the highest ionization warm absorbers.

Cloudy model predictions for the FM provide constraints on the acceleration mechanism for the absorbers. As shown in Table 1, the FMs for the UFOs are all close to unity, while the maximum value for the non-UFOs is 1.7. This indicates that the main source of opacity is electron scattering and, therefore, radiative driving will be inefficient, unless the sources are radiating at Eddington or there are multiple scatterings (see [Gofford et al. 2015](#)), which will not be possible for the predicted column densities. However, we cannot rule out the possibility that the UFOs were in a much lower ionization, hence characterized by much larger FMs, at their launch points, as noted above.

2.3. Regarding Induced Compton Scattering

As discussed above, the electron temperature in a UFO, T_e , is set by the balance of heating, due to Compton scattering, and cooling, due to inverse Compton scattering, with some

contribution from free-free scattering. If only Compton processes are involved, the electron, or “Compton”, temperature is proportional to the average photon energy (e.g., [Krolik, McKee, & Tarter 1981](#)). If the incident continuum flux is strong enough that the photon occupation number is high, and the source is anisotropic, induced Compton scattering can become important ([Kompaneets 1956](#)). Unlike inverse Compton scattering, all photon-electron interactions in induced Compton scattering result in an increase in the electron’s kinetic energy. As a result, the electron temperature can far exceed the Compton temperature ([Levich & Sunyaev 1970](#)).

Induced Compton scattering becomes important if we consider the minimum radial distances of the UFOs, r_{\min} . [Tombesi et al. \(2012\)](#) computed r_{\min} assuming that UFOs are at distances at which v_r equals the escape velocity. Under these conditions, Cloudy models predicted significant contributions from induced Compton scattering. However, Cloudy calculates the induced Compton heating based on the formalism in [Levich & Sunyaev \(1970\)](#), which is only valid if $kT_e \ll m_e c^2$, where k is Boltzmann’s constant and m_e is the electron mass. The result is that T_e will continue to increase with photon occupation number, without any physical limit. However, as discussed in [Sazonov & Sunyaev \(2001\)](#), as electrons become increasingly relativistic, the efficiency of energy transfer via induced Compton scattering drops and the maximum T_e generally will not exceed 10^9 K. Since Cloudy only considers the non-relativistic limit, the model predictions are not valid in the induced Compton regime. Therefore, we were not able to constrain the physical conditions of the UFOs at r_{\min} .

3. MAGNETO-HYDRODYNAMIC FLOWS

The physics of magneto-hydrodynamic (MHD) outflows from accretion disks has been described

in detail by BP82, for a ‘cold’ MHD flow, in which magnetic pressure exceeds gas pressure, primarily in the context of relativistic jets. For radio-quiet AGN, i.e., Seyfert galaxies, similar MHD models have been invoked to explain the dynamics of broad emission line clouds (Emmering, Blandford, & Shlosman 1992, hereafter, EBS92) and warm/UV absorbers (Bottorff et al. 2000). However, most warm absorbers are characterized by $FM \gg 1$, hence it is likely that acceleration by radiation pressure is dominant (e.g., Couto et al. 2016). On the other hand, Cloudy models predict $FM \approx 1$ for all of the UFOs and most of the non-UFOs analyzed here. As noted above, Gofford et al. (2013) suggested the possibility of radiative acceleration of UFOs via electron-scattering. This would require multiple scatterings, which would not be expected for the column densities of the UFOs, which are $< 10^{24} \text{ cm}^{-2}$. Therefore, magnetic acceleration is a possible mechanism. Also, Fukumura et al. (2014) have suggested that MHD winds can account for the properties of both UFOs and warm absorbers, in the form of a radially stratified wind.

3.1. Parameterization of cold MHD flows

The MHD wind model developed in BP82 consists of a self-similar axisymmetric flow. Self-similarity is achieved by parameterizing the cylindrical poloidal components of the position vector \mathbf{r} in such a way that flow lines, originating in the Keplerian disk at radial ‘footprint’ r_o , are easily traced (Bottorff et al. 2000). This is achieved by invoking a dimensionless free parameter χ and a dimensionless function $\xi(\chi)$ so that the position vector \mathbf{r} , in cylindrical coordinates r , ϕ , and z , is given by

$$\mathbf{r} = [r_o\xi(\chi), \phi, r_o\chi], \quad (1)$$

(BP82). By varying χ the set $(r, z) = (r_o\xi(\chi), r_o\chi)$ traces the poloidal portion of flow

streamlines (and magnetic field lines) having the footprint r_o . $\chi = 0$ corresponds to the disk plane so it is required that $\xi(0) = 1$.

As shown in BP82, the velocity vector along a flow streamline is given by:

$$\mathbf{v} = [\xi'(\chi)f(\chi), g(\chi), f(\chi)] \left(\frac{GM}{r_o} \right)^{1/2} \quad (2)$$

where the prime denotes differentiation with respect to χ , M is the BH mass, and the square-root term is the Keplerian velocity at the disk. The functions $f(\chi)$, $g(\chi)$, and $\xi(\chi)$ can be determined iteratively from the ‘cold’ MHD flow equations (see Section 2 of BP82). The flow starts in a Keplerian orbit, so $g(0) = 1$, and the initial poloidal velocity is zero, so $f(0) = 0$.

An alternative approach for finding the functions $f(\chi)$ and $g(\chi)$ is to assign $\xi(\chi)$, as in EBS92, and then $f(\chi)$ and $g(\chi)$ are found semi-analytically and self-consistently with the choice of $\xi(\chi)$ and the ‘cold’ MHD flow equations. The form of $\xi(\chi)$ used by EBS92 is:

$$\xi(\chi) = \left(\frac{\chi}{0.5 \tan \theta_o} + 1 \right)^{1/2}. \quad (3)$$

where θ_o is the launch angle of the flow with respect to the disk. This form of $\xi(\chi)$ has a value of 1 at $\chi = 0$ and gives the poloidal part of the flowlines (and magnetic field lines) a parabolic shape. While this approach limits analysis to one class of solutions possible from BP82 it illustrates relevant physical characteristics of MHD outflows so is adopted here.

To fully characterize the flow along a streamline five inputs are required: M , r_o , θ_o , λ , and κ . The constant λ is the ratio of the total, specific angular momentum, in both matter and magnetic field, to the specific angular momentum in the disk at r_o (Equations 2.2 and 2.7b of BP82). The constant κ is given by equation 3.13

of EBS92. Once $f(\chi)$ and $g(\chi)$ have been determined, the square of the Alfvén Mach number, m , is determined using equations 3.14 and 3.15 in EBS92, and the density along the streamline and the magnetic pressure, P_{mag} , are obtained from equations 3.16 and 3.17 of EBS92, respectively.

Key to constraining the input parameters are two relationships from [Bottorff et al. \(2000\)](#). The first is a linear relationship between the foot-print radius r_o and the magnitude of \mathbf{r} . The conversion from one to another is a function of angles θ_o and i , the angle between the observer’s line-of-sight and the disk axis. It can be written as:

$$r_o = |\mathbf{r}| \sin(i) \sqrt{1 + \cot^2(i) \cot^2(\theta_o) - \cot(\theta_o) \cot(i)} \quad (4)$$

The second relationship is the projected line-of-sight velocity of the flow:

$$v_{\text{obs}} = \left[\xi'(\chi) f(\chi) \sin i + f(\chi) \cos i \right] \sqrt{\frac{GM}{r_o}}. \quad (5)$$

If we have constraints on M and i and $|\mathbf{r}|$, we can obtain the footprint radius, r_o for a given θ_o . Then with M , i , and r_o , and v_{obs} , we can determine the value of $f(\chi)$ (at the location of the UFO). But along the line-of-sight $\chi = z/r_o = |\mathbf{r}| \cos(i)/r_o$, so χ is determined. The input parameters λ and κ can be adjusted until the model reproduces the observationally inferred $f(\chi)$ at the observationally inferred χ . This fixes the flow solution enabling estimation of the spatial extent of the absorption system, given the velocity width of observed spectral features and the column density. In the next subsection, we apply this form of a “cold” MHD solution to the UFO in NGC 4151, for which we use values for M and i from previous studies and the constraint on $|\mathbf{r}|$ from our photo-ionization analysis.

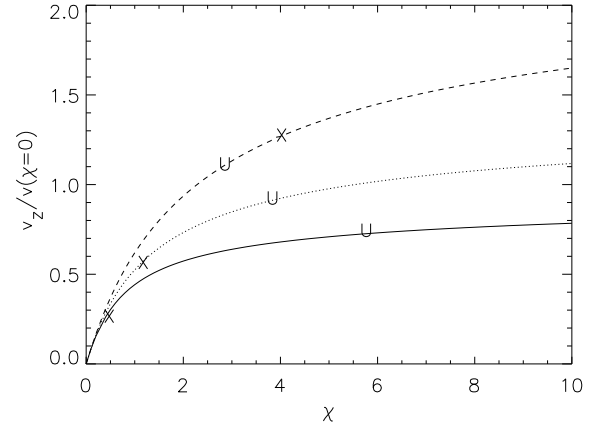


Figure 3. The ratio of v_z to the Kelperian velocity at the footprint of the flow, plotted against χ , for launch angles $\theta_o = 20^\circ$ (solid), 30° (dotted), and 40° (dashed). The Alfvén critical points (X) and position of the UFO (U) are indicated for all three. Note that for $\theta_o = 40^\circ$, the UFO is at a sub-Alfvénic point.

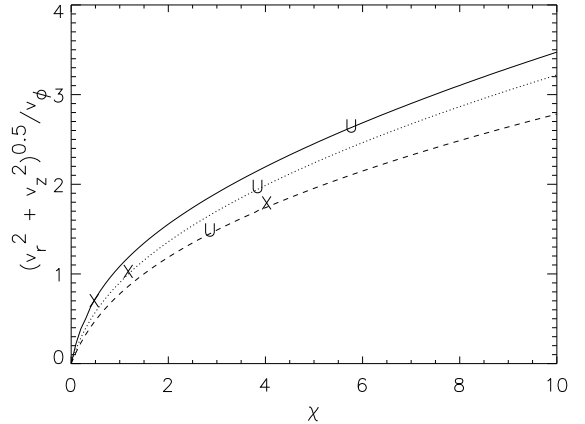


Figure 4. The ratio of the poloidal to the azimuthal components of velocity, plotted against χ , for all θ_o , as in Figure 4. The Alfvén critical and UFO positions are indicated.

3.2. NGC 4151: a Case Study

While MHD models have been successful in predicting the general properties of warm absorbers (e.g., Proga 2000) and UFOs (Fukumura et al. 2014), there have not been any tight constraints on critical parameters, such as density, location, and magnetic field strengths, based on observational analysis. We are now able to do so in the case of NGC 4151, for which we have constraints on the properties of the UFO and the inclination of the accretion disk.

Based on the constraint $\Delta r/r < 1$, the maximum radial distance for the UFO in NGC 4151 is $r = 3.2 \times 10^{15}$ cm (see Table 1). We also use an inclination of $\sim 45^\circ$ (Das et al. 2005) and a black hole mass $M = 4.57 \times 10^7 M_\odot$ (Bentz et al. 2006).

3.2.1. Predicted Properties of the Flow

To characterize the flow, we use the method outlined in Section 3.1 to calculate the foot-print radius as a function of launch angle and the flow scaling parameters at the position of the UFO. In Table 3, we give the values of parameters characterizing the flows for launch angles $\theta_o = 20^\circ, 30^\circ, \text{ and } 40^\circ$. For a given inclination, as launch angle increases, the radial distance of the footprint increases. However, the position along the flow where the streamline intersects our line-of-sight decreases, as evidenced by the decrease in χ_{UFO} . In Figures 3 through 9, the physical parameters of the flow for the different values of θ_o , are plotted against χ .

As shown in Figure 3, the ratio of v_z to the Kelperian velocity at the footprint increases with χ along the streamline, eventually reaching the asymptotic values, f_∞ , listed in Table 3. In Figure 4, the ratio of the poloidal component of the flow, $\sqrt{v_r^2 + v_z^2}$, to the azimuthal component, v_ϕ , as a function of χ , is shown for $\theta_o = 20^\circ, 30^\circ$ and 40° . For each θ_o , the flow becomes increasingly poloidal with increasing χ . Note that for $\theta_o = 40^\circ$, the outflow is sub-

Alfvénic at the position of the UFO. This is the result of a greater magnetic field strength compared to the other cases (see below).

The density, ρ , relative to that at the Alfvén critical point, is shown in Figure 5. As shown in EBS92, ρ decreases with increasing m . For a given χ , m is smaller for larger θ_o . This is largely due to the value of κ (see, Table 3 and EBS92, Equation 3.15), hence, ρ/ρ_A is greater for smaller launch angles. This is clearly evident for $\theta_o = 40^\circ$, when the UFO lies below the Alfvén critical point, as noted above. In Figure 6, we plot P_{mag} relative to that at the Alfvén critical point. Again, the values for different θ_o can be understood in terms of m and the proximity of the UFO relative to the critical point.

Since the flow velocity depends on the magnetic field strength, it is instructive to compare the magnetic pressure with energy density. Rees (1987) suggested that the broad emission-line region (BLR) clouds in AGN are magnetically confined and, furthermore, that there is equipartition between the magnetic field and gravity. If so, the magnetic pressure and the gravitational energy density should be roughly equal, or

$$P_{\text{mag}} \approx \frac{GM\rho}{r}. \quad (6)$$

In its role in cloud-confinement, the B field is not directly affecting the BLR dynamics. However, in the case of an MHD wind, the B field is the mechanism that drives the outflow, and, therefore, there is no reason to expect equipartition.

In Figures 7 - 9, we show the ratio of P_{mag} to gravitational energy density. In each case, conditions are close to equipartition near the footprint. For $\theta_o = 20^\circ$, the ratio rises, but the flow stays close to equipartition. However, at greater θ_o the ratio rapidly exceeds equipartition. This

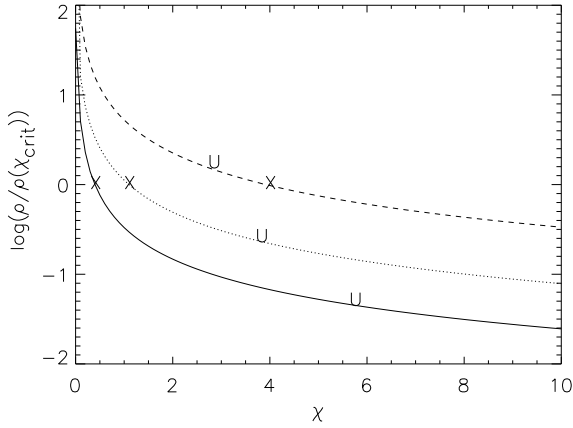


Figure 5. Density relative to that at the Alfvén critical point, as a function of χ for $\theta_o = 20^\circ$ (solid), 30° (dotted), and 40° (dashed).

is consistent with the corresponding greater B field strengths (see Table 4).

A larger θ_o means that the field lines are more coiled on top of one another. The field must be strong enough to buoy a vertical column of out-flowing material in the MHD wind. As shown in Table 4, all components of the B field are greater at the position of the UFO, the toroidal component, B_ϕ , increases the most with larger θ_o , as expected.

In Figures 7-9, we also show the ratio of P_{mag} to the kinetic energy density, $\frac{1}{2}\rho v_{\text{tot}}^2$, where v_{tot}^2 is the sum of the squares of the poloidal and toroidal components of velocity. For each θ_o , the ratio is relatively flat, which is consistent with the dependence of both quantities on m . Finally, in Table 4 we list the log of the ratio of P_{mag} to the gas pressure, P_{gas} , at the position if the UFO. In each case, $P_{\text{mag}} \gg P_{\text{gas}}$, which is consistent with a cold MHD flow.

3.2.2. Constraints on Velocity Structure

The UFO detected in the *XMM* observation of NGC 4151 was resolved, with a dispersion of

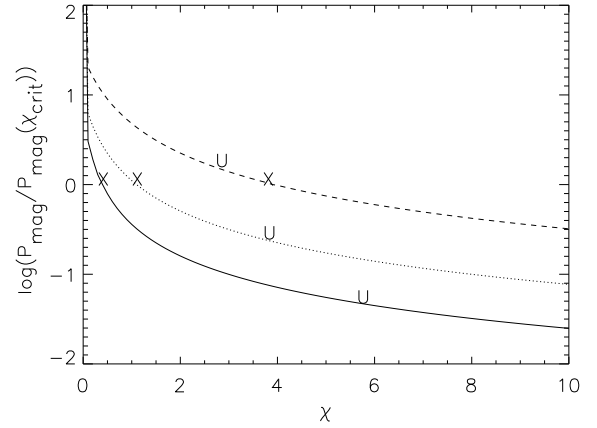


Figure 6. Magnetic pressure relative to that at the Alfvén critical point, as a function of χ , for $\theta_o = 20^\circ$ (solid), 30° (dotted), and 40° (dashed).

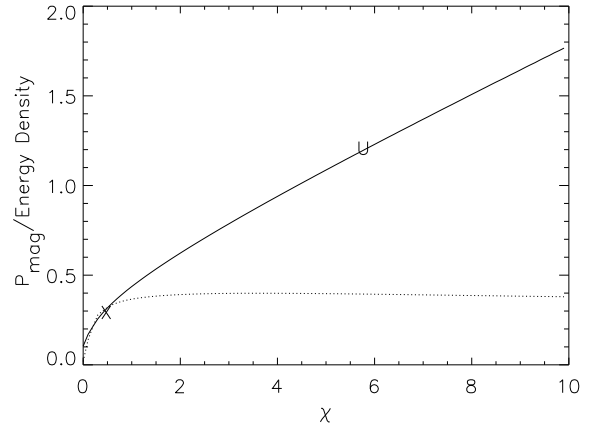


Figure 7. The ratios of magnetic pressure to gravitational energy density (solid) and kinetic energy density (dotted), as a function of χ for $\theta_o = 20^\circ$.

$\sigma = 5.1(+1.8/-1.4) \times 10^3 \text{ km s}^{-1}$, or Full Width at Half Maximum ($FWHM$) = $1.2(+0.4/-0.3) \times 10^4 \text{ km s}^{-1}$ (Tombesi et al. 2010). As noted above, Tombesi et al. (2011) fit the spectrum with XSTAR models by including microturbulence. Bottorff & Ferland (2000) sug-

Table 1. Model Predicted Properties

name	r	log Xi	log N_H	log n_H	log T	HC ^a	FM
	cm		cm ⁻²	cm ⁻³	K	%	
(1)	(2)	(3)	(4)	(5)	(6)	(7)	(8)
UFOs							
NGC 4151	15.5	4.33	22.9	7.4	7.32	96.5	1.01
IC 4329a	16.1	4.87	23.1	7.1	7.45	99.0	1.00
Mrk 509 obs1	15.8	5.16	23.9	7.5	7.49	99.4	1.00
Mrk 509 obs2	15.7	5.15	23.6	7.7	7.49	99.4	1.00
Mrk 509 obs3	16.5	4.25	23.7	7.3	7.28	95.1	1.01
Ark 120	16.3	4.55	23.7	7.5	7.39	97.8	1.00
Mrk 79	16.5	4.19	23.1	6.7	7.25	94.8	1.01
NGC 4051 obs1	14.9	4.37	23.0	8.1	7.34	96.9	1.01
Mrk 766 obs1	17.1	3.73	22.4	5.3	6.88	81.3	1.06
Mrk 766 obs2	15.9	4.28	23.0	7.3	7.29	96.0	1.01
Mrk 841	17.0	3.91	23.0	6.0	7.05	88.5	1.03
Mrk 290	16.3	3.91	23.4	7.1	7.05	87.9	1.03
Mrk 205	15.7	4.62	23.8	8.1	7.42	98.1	1.00
MCG-5-23-16	16.6	4.25	22.7	6.1	7.28	95.7	1.01
NGC 4507	15.9	4.53	23.0	7.1	7.39	97.9	1.00
non-UFOs							
Mrk 279	17.9	3.33	22.2	5.0	6.34	46.9	1.32
NGC 3516 obs1	16.6	3.73	22.5	5.9	6.87	81.3	1.06
NGC 3516 obs2	16.8	3.76	22.5	6.4	6.90	82.7	1.05
NGC 3783 obs1	18.0	3.13	22.5	4.5	6.09	24.4	1.73
NGC 3783 obs2	17.8	3.23	22.4	4.6	6.20	33.7	1.45
NGC 3783 obs3	18.0	3.13	22.5	4.5	6.09	24.4	1.73
ESO 323-G77	17.0	3.53	23.5	6.5	6.62	65.3	1.12

^aHC is the fractional contribution of Compton Heating.

Table 2. Log Fe Column Densities

name	Fe ⁺²³	Fe ⁺²⁴ (mes ^a)	Fe ⁺²⁵ (mes ^a)
	cm ⁻²	cm ⁻²	cm ⁻²
UFOs			
NGC 4151	14.4	16.6	17.7 (17.9)
IC 4329a	12.8	15.6	17.4 (17.3)
Mrk 509 obs1	13.0	16.0	18.0 (17.9)
Mrk 509 obs2	12.5	15.5	17.6 (17.6)
Mrk 509 obs3	15.7	17.7	18.7
Ark 120	14.6	17.0	18.4
Mrk 79	15.2	17.2	18.1 (18.0)
NGC 4051 obs1	14.3	16.6	17.8
Mrk 766 obs1	16.1	17.4	17.7 (18.0)
Mrk 766 obs2	14.6	16.7	17.8 (17.8)
Mrk 841	16.1	17.7	18.2
Mrk 290	16.6	18.1	18.6
Mrk 205	14.5	17.0	18.4 (18.3)
MCG-5-23-16	14.5	16.6	17.6 (17.6)
NGC 4507	13.8	16.2	17.6
non-UFOs			
Mrk 279	17.1	17.5 (17.5)	17.0
NGC 3516 obs1	16.2	17.5 (17.5)	17.8 (17.8)
NGC 3516 obs2	16.1	17.5 (17.3)	17.8 (17.7)
NGC 3783 obs1	17.3	17.4 (17.4)	16.5
NGC 3783 obs2	17.3	17.6 (17.6)	16.9
NGC 3783 obs3	17.3	17.4 (17.4)	16.5
ESO 323-G77	18.0	18.8 (18.8)	18.6 (18.4)

^ames refers to the column densities derived from curve-of-growth (Section 2.1).

Table 3. Flow Parameters for NGC 4151

θ_o	χ_{UFO}	χ_A	f_{UFO}	f_∞	λ	κ	$\log(r_o)$ (cm)	$\log(v_o)$ (cm s ⁻¹)
(1)	(2)	(3)	(4)	(5)	(6)	(7)	(8)	(9)
20°	5.64	0.36	0.73	0.98	2.95	2.10	14.59	9.59
30°	3.71	1.06	0.91	1.46	4.68	0.65	14.77	9.51
40°	2.73	3.91	1.08	2.42	10.3	0.14	14.91	9.43

Table 4. Magnetic Properties^a

θ_o	B_z^b	B_r	B_ϕ	B_{tot}	$\log(P_{\text{mag}}/P_{\text{gas}})$
(1)	(2)	(3)	(4)	(5)	(6)
20°	12.9	6.2	46.3	48.4	2.76
30°	31.6	14.7	110.3	115.7	3.52
40°	83.6	36.5	360.4	371.8	4.53

^aEvaluated at r_{UFO} .

^b B_i is the i-component of the magnetic field in units of G.

gested that the smoothness of BLR emission-lines were the result of micro-turbulence and that turbulent BLR clouds could exist if magnetically confined. Hence, in the presence of strong B fields, such as those calculated in the MHD modeling, it is possible that the UFOs are highly turbulent.

On the other hand, a large $FWHM$ can result from a large velocity gradient along our line-of-sight through the absorbing material. This scenario was discussed in detail in [Bottorff et al. \(2000\)](#). Here we use their Equation 14, reformatted in terms of $\Delta r/r$. This allows for more direct comparison of the MHD model kinemat-

ics to our photo-ionizing model results. The relationship is:

$$\frac{\Delta r}{r} = 4 \left(\frac{\Delta v}{2v_r} \right) \left[1 - \left(\frac{\Delta v}{2v_r} \right)^2 \right]^{-2} \quad (7)$$

where Δv is $FWHM$, and v_r is the radial velocity of the UFO. From this, $\Delta r/r \approx 0.8$, which is consistent with the constraint on the Cloudy models that $\Delta r/r \leq 1$ (see Section 2.1). This can occur if our line-of-sight passes through streamlines originating at different launch radii (see [Bottorff et al. 2000](#), Figure 1). We suggest that the observed $FWHM$ is more likely due to a radial velocity gradient, rather than micro-turbulence.

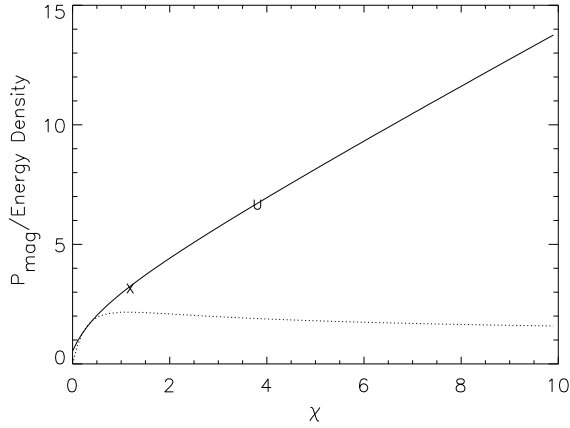


Figure 8. The ratios of magnetic pressure to gravitational energy density (solid) and kinetic energy density (dotted), as a function of χ for $\theta_o = 30^\circ$.

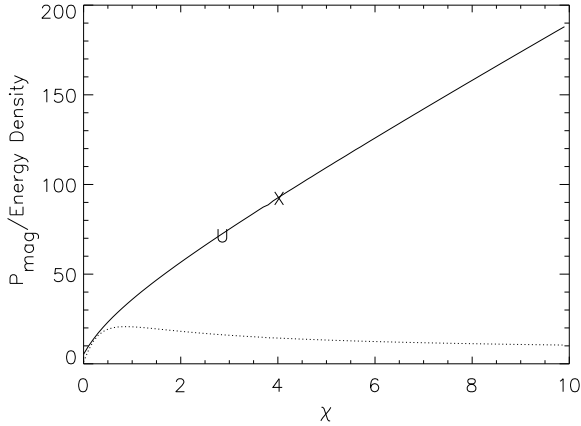


Figure 9. The ratios of magnetic pressure to gravitational energy density (solid) and kinetic energy density (dotted), as a function of χ for $\theta_o = 40^\circ$.

4. DISCUSSION

As shown in the previous section, the UFO in NGC 4151 can be characterized as part of a cold MHD flow, with an origin in the accretion disk. Mass outflow has been well-studied

in NGC 4151 (e.g., [Crenshaw et al. 2015](#)), and we have constraints on the physical conditions and radial distances of the various components of absorption ([Kraemer et al. 2005](#)). Therefore, we are able to consider the UFO in the context of mass outflow in this source.

As discussed in [Kraemer et al. \(2005, 2006\)](#) and [Couto et al. \(2016\)](#), there are two main components of absorption in NGC 4151: “XHIGH”, which was initially detected by the presence of Mg XII, S XIV, and S XVI absorption lines, and D+Ea, which causes the broad-band soft X-ray absorption and has a UV signature in the form of saturated C IV, N V, and O VI lines. Even though most of the *Chandra* and *XMM-Newton* observations of NGC 4151 found the source in very low-flux states, with $L_{\text{bol}}/L_{\text{Edd}} \sim$ a few percent, [Couto et al. \(2016\)](#) demonstrated that D+Ea could be radiatively accelerated. However, XHIGH was too highly ionized for radiative acceleration in a sub-Eddington source, hence it could be MHD-driven.

[Fukumura et al. \(2014, and references therein\)](#) suggest that an MHD-driven disk wind will result in a continuous distribution of N_{H} per decade of ionization parameter, which results in a density law of the form $n(r) \propto r^{-\alpha}$, where $\alpha \sim 1$. As discussed in [Couto et al. \(2016\)](#), the similar values of N_{H} for D+Ea, XHIGH, and the UFO are consistent with this scenario. However, the density and location of D+Ea relative to the UFO yields $\alpha \sim 0.5$, which is inconsistent with [Fukumura et al. \(2014\)](#)’s requirement for MHD. Based on photo-ionization modeling, [Kraemer et al. \(2005\)](#) argued that XHIGH must be closer to the continuum source than D+Ea, and [Couto et al. \(2016\)](#) determined that the conditions in XHIGH are in agreement with the MHD model proposed by [Fukumura et al. \(2014\)](#). Overall, this picture is suggestive of stratification of the outflow in which the interior sections are MHD-driven while, at sufficiently

large radial distances, radiation-driving dominates. Also, XHIGH’s properties overlap the lower ionization end of the non-UFOs. Hence, one can envision a scenario in which UFOs are launched at the smallest radii and non-UFOs, while still MHD-driven, form further out. This is consistent with our photo-ionization modeling analysis (see Table 1).

Comparing XMM-Newton (Tombesi et al. 2010, 2011) and Suzaku (Gofford et al. 2015) observational results, there are cases of large velocity differences occurring on relatively short timescales. For example, for the UFO in NGC 4151, Tombesi et al. (2010) found $v_{\text{obs}}/c = 0.106 \pm 0.007$, while, in a Suzaku spectra taken ~ 18 days later, Gofford et al. (2015) found $v_{\text{obs}}/c = 0.055 \pm 0.023$. A more extreme difference was seen in Mrk 279, with $v_{\text{obs}}/c < 0.007$ (Tombesi et al. 2011) versus 0.222 ± 0.006 , approximately 3.5 yrs later (Gofford et al. 2015). In the case of NGC 4151, the difference in v_{obs} might be consistent with a change in the direction of the velocity vector, as suggested for a component of UV absorption in NGC 3783 (Gabel et al. 2003), but such a scenario would require a small covering factor for the UFO, which seems unlikely given its large column density and the possibility that our line-of-sight passes through different streamlines, as discussed above. We suggest that it is more plausible that these are individual components of absorption, whose velocity differences result from different launch radii or different physical conditions, such as the magnetic field strengths, at the times of ejection.

Other than NGC 4151, there do not appear to be sources that harbor UFOs and non-UFOs, at least in the same epoch. Based on our model constraints, the non-UFOs are at larger distances (see Table 1), which implies that the may have originated at larger r_o . In the context of an MHD outflow, the lower values of

v_r are consistent with lower Kelperian velocities at the launch points, hence lower outflow velocities. However, this does not explain why the two types cannot be present in the same objects. One possibility is that the conditions in the disk are such that either UFOs or non-UFOs are created. If this is related to magnetic field strength, there may be associated changes in the core radio emission.

Crenshaw & Kraemer (2012) found that $L_{\text{KE}} = 0.25$ to 1.6×10^{41} erg s $^{-1}$, or 0.34 to $2.0 \times 10^{-3}L_{\text{bol}}$, for the combined UV and X-ray absorbers in NGC 4151. Including the optical/UV NLR emission line gas increases L_{KE} to a peak of 4.3×10^{41} erg s $^{-1}$ (0.006 - 0.008 of L_{bol}). This is barely sufficient for feedback. Based on our characterization of the UFO, we obtain $L_{\text{KE}} = 3.5 \times 10^{43}$ erg s $^{-1}$, for $C_g = 0.5$, which is on the same order as L_{bol} . Therefore, if the UFO has a large covering factor, and can maintain its integrity as it moves into the galactic bulge, it has sufficient kinetic luminosity for effective AGN feedback.

If MHD-driven UFOs play an important role in AGN feedback, the interaction between the SMBH and the host galaxy is via the magnetic properties of the disk. This is opposed to feedback due to radiatively-driven winds, which is the more typically invoked scenario. Interestingly, the cold MHD model discussed by BP82 was intended to explain radio jets. Therefore, the form of “UFO feedback” we describe in the present paper is simply a less energetic form of the same phenomenon. Since UFOs can form in sub-Eddington sources, which do not seem to be able to produce the high L_{KE} winds required for feedback, perhaps a more broadly defined radio mode feedback, which includes UFOs, is the dominant means of SMBH/host interaction.

5. CONCLUSIONS

Starting with a sample of AGN with intrinsic Fe XXV and Fe XXVI absorption detected by *XMM-Newton* (Tombesi et al. 2010, 2011), we have analyzed the physical conditions within the absorbers, using photo-ionization models generated with *Cloudy* (Ferland et al. 2013). We have determined the following:

1. It has been shown that there is a continuum of properties, with decreasing ionization and (generally) column density, over the range from UFOs to non-UFOs to warm absorbers (e.g., Tombesi et al. 2011). The highest ionization warm absorbers appear to overlap the non-UFO region, which suggests there may be some connection between these phenomena. We have shown that UFOs and non-UFOs occupy different regions on an S-curve, with little overlap, with the former in the Compton-dominated range, while the latter are in the vertical range, where other cooling mechanisms become important. Based on our model constraints, the non-UFOs lie at greater radial distances than the UFOs. Overall, this is consistent with $n_{\text{H}} \propto r^{-\alpha}$, with $\alpha < 2$, in which case the ionization state of the absorbers decreases with distance, with an associated change in the heating and cooling processes.
2. *Cloudy* models predict that UFOs and non-UFOs are characterized by $\text{FM} \sim \text{unity}$ hence they are too highly ionized to be radiatively accelerated in sub-Eddington sources, unless the UFOs were in a much lower ionization state at their launch points. This suggests another means of acceleration, such as an MHD-driven flow.
3. To explore the possibility of MHD-driving, we applied the cold MHD model detailed in BP82 and EBS92 to case of NGC 4151, for which the inclination of the black hole/accretion disk has been constrained (Das et al. 2005). Specifically, we followed the flow parameterization in EBS92, for which the poloidal part of the

streamlines are parabolic, with a footprint in the accretion disk. For a range of launch angles, we find that the observed velocity is consistent with MHD acceleration along a streamline and we are able to trace the origin of the UFO back to its footprint radius. Also, with this geometry, the observed the relationship between the *FWHM* and v_{obs} of the UFO in NGC 4151 is consistent with a velocity gradient through different flow streamlines.

4. For NGC 4151 we have been able to constrain the magnetic field strength and magnetic pressure in the flow. We find that magnetic pressure far exceeds gas pressure predicted by the *Cloudy* models, consistent with the definition of a cold flow. Also, the magnetic pressure generally exceeds the gravitational energy density, therefore equipartition does not apply.

Given the simplicity of this model, such as the assumptions of rigid field lines and parabolic geometry, we do not suggest that these results be taken as the final word on MHD-driven outflows. Rather, the physical parameters, such as density and magnetic field strength along the streamlines, will be useful inputs to more sophisticated models, such as those developed by Fukumura et al. (2014). However, if, as we suggest, these outflows are magnetically driven disk-winds, understanding their variability and the different origins of UFOs and non-UFOs may provide new insight into the physics of accretion disks in AGN. It would be particularly interesting if there was a connection between UFO properties and the radio emission from these objects. Finally, if UFOs are an important feedback mechanism, particularly in sub-Eddington AGN, it implies that magnetic properties of the disk can affect the host galaxy, as is the case for radio-mode feedback.

6. ACKNOWLEDGMENTS

We thank E. Behar, D. Kazanas, K. Fukumura, C. Shrader, D. Proga, and M. Rees for useful comments and suggestions. We also thank

G. Ferland and associates for their continuing maintenance of Cloudy. F.T. acknowledges support from the Programma per Giovani Ricercatori - anno 2014 “Rita Levi Montalcini”.

REFERENCES

- Asahina, Y., Nomura, M., & Oshuga, K. 2017, *ApJ*, 840, 25
- Asplund, M., Grevesse, N., & Sauval, A. J. 2005, in *Astronomical Society of the Pacific Conference Series*, Vol. 336, *Cosmic Abundances as Records of Stellar Evolution and Nucleosynthesis*, ed. T. G. Barnes, III & F. N. Bash, 25
- Begelman, M. C. 2004, in *Coevolution of Black Holes and Galaxies*, ed. L. C. Ho (Cambridge: Cambridge Univ. Press), 374
- Begelman, M. C., McKee, C. F., & Shields, G. A. 1983, *ApJ*, 271, 70
- Bentz, Misty C., Denney, Kelly D., Cackett, Edward M., Dietrich, Matthias, Fogel, Jeffrey K. J., Ghosh, Himel, Horne, Keith, Kuehn, Charles, Minezaki, Takeo, Onken, Christopher A., et al. 2006, *ApJ*, 651, 775
- Blandford, R. D., & Payne, D. G. 1982, *MNRAS*, 199, 883
- Bottorff, M. C., Korista, K. T., & Shlosman, I. 2000, *ApJ*, 537, 1346
- Bottorff, M. C., & Ferland, G. J. 2000, *MNRAS*, 316, 103
- Cappi, M., Panessa, F., Bassani, L., Dadina, M., Di Cocco, G., Comastri, A., della Ceca, R., Filippenko, A. V.; Gianotti, F., Ho, L. C., et al. 2006, *A&A*, 446, 459
- Cappi, M., Tombesi, F., Bianchi, S., Dadina, M., Giustini, M., Malaguti, G., Maraschi, L., Palumbo, G. G. C., Petrucci, P. O., Ponti, G. et al. 2008, *A&A*, 504, 401
- Chakraborty, S., Petrucci, P.-O., Ferreira, J., et al. 2016, *A&A*, 589, A119
- Chartas, G., Brandt, W. N., & Gallagher, S. A. 2003, *ApJ*, 595, 85
- Couto, J. D., Kraemer, S. B., Turner, T. J., & Crenshaw, D. M. 2016, *ApJ*, 833, 191
- Crenshaw, D. Michael, Kraemer, Steven B., Boggess, Albert, Maran, Stephen P., Mushotzky, Richard F., & Wu, Chi-Chao 1999, *ApJ*, 516, 750
- . 2012, *ApJ*, 753, 75
- Crenshaw, D. M., Kraemer, S. B., & George, I. 2003, *ARA&A*, 41, 117
- Crenshaw, D. M., Fischer, T. C., Kraemer, S. B., & Schmitt, H. R. 2015, *ApJ*, 799, 83
- Das, V., Crenshaw, D. M., Hutchings, J. B., Deo, R. P., Kraemer, S. B., Gull, T. R., Kaiser, M. E., Nelson, C. H., & Weistrop, D. 2005, *AJ*, 130, 945
- Dunn, Jay P., Crenshaw, D. Michael, Kraemer, S. B., & Gabel, J. R. 2007, *AJ*, 134, 1061
- Emmering, Robert T., Blandford, Roger D., & Shlosman, Isaac 1992, *ApJ*, 385, 460
- Ferland, G. J., Porter, R. L., van Hoof, P. A. M., et al. 2013, *RMxAA*, 49, 137
- Feruglio, C., Fiore, F., Carniani, S., Piconcelli, E., Zappacosta, L., Bongiorno, A., Cicone, C., Maiolino, R., Marconi, A., Menci, N. et al. 2015, *A&A*, 583, 99
- Fischer, Travis C., Machuca, C., Diniz, M. R., et al. 2017, *ApJ*, 834, 30
- Fukumura, Keigo, Kazanas, Demosthenes, Contopoulos, Ioannis, & Behar, Ehud 2010, *ApJ*, 723, L228
- Fukumura, Keigo, Tombesi, Francesco, Kazanas, Demosthenes, Shrader, Chris, Behar, Ehud & Contopoulos, Ioannis 2014, *ApJ*, 780, 120
- Gabel, Jack R., Crenshaw, D. Michael, Kraemer, Steven B., Brandt, W. N., George, Ian M., Hamann, Frederick W., Kaiser, Mary Elizabeth, Kaspi, Shai, Kriss, Gerard A.; Mathur, Smita, et al. 2003, *ApJ*, 595, 120
- Gofford, J., Reeves, J. N., McLaughlin, D. E., Braitto, V., Turner, T. J., Tombesi, F., & Cappi, M. 2015, *MNRAS*, 451, 4169
- Gofford, J., Reeves, J. N., Tombesi, F., Braitto, V., Turner, T. J., Miller, L., & Cappi, M. 2013, *MNRAS*, 430, 60
- Hagino, Kouichi, Done, Chris, Odaka, Hirokazu, Watanabe, Shin, Takahashi, Tadayuki, 2017, *MNRAS*, 468, 1442

- Hagino, Kouichi, Odaka, Hirokazu, Done, Chris, Gandhi, Poshak, Watanabe, Shin, Sako, Masao, Takahashi, Tadayuki 2015, MNRAS, 446, 663
- Hopkins, Philip F., & Elvis, Martin 2010, MNRAS, 401, 7
- Kaasra, J.S., Mewe, R., Liedahl, D.A., Komossa, S., & Brinkman, A.C. 2000, A&A, 354, L83
- Kallman, T. R., Palmeri, P., Bautista, M. A., Mendoza, C., & Krolik, J. H. 2004, ApJS, 155, 675
- Kaspi, Shai, Brandt, W. N., Netzer, Hagai, Sambruna, Rita, Chartas, George, Garmire, Gordon P., & Nousek, John A. 2004, ApJ, 535, L17
- King, Andrew, & Pounds, Ken 2015, ARA&A, 53, 115
- Kompaneets, A. S. 1956, Soviet Phys. JETP, 4, 730
- Kraemer, S. B., Crenshaw, D. M., Gabel, J. R., Kriss, G. A., Netzer, H., Peterson, B. M., George, I. M., Gull, T. R., Hutchings, J. B., Mushotzky, R. F., & Turner, T. J. 2006, ApJS, 167, 161
- Kraemer, S. B., George, I. M., Crenshaw, D. M., Gabel, J. R., Turner, T. J., Gull, T. R., Hutchings, J. B., Kriss, G. A., Mushotzky, R. F., Netzer, H., Peterson, & B. M., Behar, E. 2005, ApJ, 633, 693
- Kraemer, S. B., Sharma, N., Turner, T. J., George, Ian M., & Crenshaw, D. Michael 2015, ApJ, 798, 53
- Krolik, J. H., McKee, C. F., & Tarter, C. B. 1981, ApJ, 249, 422
- Laor, Ari, Fiore, Fabrizio, Elvis, Martin, Wilkes, Belinda J., & McDowell, Jonathan C. 1997, ApJ, 477, 93
- Levich, E. V., & Sunyaev, R. A. 1970, Astrophysical Letters, 7, 69
- Murray, N, Chiang, J., Grossman, S. A., & Voit, G. M. 1995, ApJ, 451, 498
- Nardini, E., Reeves, J. N., Gofford, J., Harrison, F. A., Risaliti, G., Braitto, V., Costa, M. T., Matzeu, G. A., Walton, D. J., Behar, E., et al. 2015, Sci, 347, 860
- Nomura, M, & Ohsuga, K. 2017, MNRAS, 465, 2873
- Nomura, Mariko, Ohsuga, Ken, Takahashi, Hiroyuki R., Wada, Keiichi, & Yoshida, Tessei 2016, PASJ, 68, 16
- Pounds, K. A., & Reeves, J. N. 2009, MNRAS, 397, 249
- Pounds, K. A., Reeves, J. N., King, A. R., Page, K. L., O'Brien, P. T., & Turner, M. J. L. 2003, MNRAS, 345, 705
- Proga. Daniel 2000, ApJ, 538, 684
- Reeves, J. N., Braitto, V., Nardini, E., Behar, E., O'Brien, P. T., Tombesi, F., Turner, T. J., & Costa, M. T. 2016, ApJ, 824, 20
- Rees, M. J. 1987, MNRAS, 228, P47
- Reeves, James, Done, Chris, Pounds, Ken, Terashima, Yuichi, Hayashida, Kiyoshi, Anabuki, Naohisa, Uchino, Masahiro, Turner, Martin. 2008, MNRAS, 385, L108
- Reeves, J. N., O'Brien, P. T., & Ward, M. J. 2003, ApJ, 593, L65
- Sazonov, S. Yu., & Sunyaev. R. A. 2001, Astronomy Letters, 27, 481
- Scannapieco, Evan, & Oh, S. Peng 2004, ApJ, 608, 62
- Takeuchi, Shun, Ohsuga, Ken, & Mineshige, Shin 2013, PASJ, 65, 88
- Tarter, C. Bruce, Tucker, Wallace H., & Salpeter, Edwin E. 1969, ApJ, 156, 943
- Tombesi, F. Melédez, M., Veilleux, S., Reeves, J. N., González-Alfonso, E., & Reynolds, C. S. 2015, Nature, 519, 436
- Tombesi, F., Tazaki, F., Mushotzky, R. F., Ueda, Y., Cappi, M., Gofford, J., Reeves, J. N., & Guainazzi, M. 2014, MNRAS, 443, 2154
- Tombesi, F., Cappi, M., Reeves, J. N., Nemmen, R. S., Braitto, V., Gaspari, M., & Reynolds, C. S. 2013, MNRAS, 430, 1102
- Tombesi, F., Cappi, M., Reeves, J. N., & Braitto, V. 2012, MNRAS, 422, L1
- Tombesi, F., Cappi, M., Reeves, J. N., Palumbo, G. G. C., Braitto, V., & Dadina, M. 2011, ApJ, 742, 44
- Tombesi, F., Cappi, M., Reeves, J. N., Palumbo, G. G. C., Yaqoob, T., Braitto, V., & Dadina, M. 2010, A&A, 521, 57
- Wagner, A.Y, Umemura, M., & Bicknell, G. V. 2013, ApJL, 763, L18